Comparative Analysis of Rotating Electrode and Gas Diffusion Electrode Methods for Assessing Activity and Stability of Fe-N-C Based Catalysts in ORR

*Marco Mazzucato and Christian Durante**

Department of Chemical Sciences, University of Padova, via Marzolo 1, 35131, Padova, Italy.

*christian.durante@unipd.it

Abstract

Rotating (ring) disk electrode (R(R)DE) voltammetry is considered a simple means of benchmarking the oxygen reduction reaction (ORR) activity of platinum-free electrocatalysts for proton exchange membrane fuel cells or hydrogen peroxide electrocatalysts. However, the R(R)DE methodology has shown high variability across laboratories and reproducible ORR activities can be obtained when a strict experimental protocol is followed. Despite this, objections in the literature have been raised regarding the usefulness of screening measurements on RRDEs in identifying a good catalyst that maintains the same performance when switching from the RRDE to a gas diffusion electrode (GDE). As a result, new experimental approaches have been proposed in the literature to better evaluate a catalyst under conditions similar to those of a fuel cell or an electrolyzer. Our study, along with others, points out that even with a new electrochemical set-up, the dominant factors in the screening experimental protocol include the ink formulation, electrocatalyst film quality, and electrochemical procedures.

In this study, a platinum-free Fe-N-C type catalyst (Fe2XC72) is considered a benchmark electrocatalyst for ORR. The activity and selectivity performances of the catalyst are evaluated and compared on an RRDE, a half-cell with a GDE electrode, and an H-cell with a GDE electrode but with a larger surface area. The impact of various experimental parameters, including catalyst loading and pH, on the electrocatalytic activity and selectivity, are evaluated and the different techniques,

although not completely comparable, manage on individual aspects to produce similar if not overlapping results. Furthermore, explicit experimental procedures and measurement protocols are reviewed and revised.

Keywords: PGM-free, electrocatalysis, ORR, GDE, H_2O_2, PEMFC

1 Introduction

The electrochemical characterization of metal nitrogen carbon (M-N-C; M = Fe, Mn, Co, etc.) materials for oxygen reduction reaction (ORR) has been widely explored using rotating (ring) disc electrode (R(R)DE) configuration since it allows to obtain a rapid evaluation of both activity and selectivity. The typical RDE configuration consists of a glassy carbon (GC) disc on which the catalyst is drop-casted. It was well recognized in the literature that the carbon loading on the electrode [1], the amount of ionomer [2], the solvent, or the carbon grinding method are parameters extremely complicated to control so an optimization of the experimental conditions should be done for each material studied [3]. GC is an ideal electrode support since it is stable over a large potential window and almost inert versus the oxygen reduction, so the surface response, when a material is cast on it, is solely due to the catalyst and not to the GC surface. Researchers take advantage of the steady-state laminar flow conditions adjacent to an RDE or RRDE to carefully gather information about electrode reaction kinetics. ORR activity is usually measured by linear sweep voltammetry (LSV) with scan rates equal to or below 20 mV s^{-1} to minimize capacitive currents even if background subtraction is always advisable, especially with M-N-C catalysts where capacity current can be dominating. Several guiding papers in the literature provide methods to accurately and reproducibly determine the activity of Pt-based electro-catalysts for the oxygen reduction reaction in proton exchange membrane fuel cells (PEMFC) [4–7]. Much fewer papers are available on the characterization of PGM-free catalysts [8]. Besides the practical advantages, the R(R)DE set-up has also several drawbacks, since the

experimental conditions are always far from a real device, for example, the limiting mass transport regime, the catalysts loading, and film thickness. For this reason, it is mandatory to idealize a simpler setup that is closer to the real device, and significant progress has been made in this field over the last decade. For example, Kucernak and Co. developed a new floating electrode technique (FET) where the ink is applied onto a porous Au-coated polycarbonate membrane floating on the electrolyte. Oxygen can reach the catalyst directly through the membrane pores from the gas phase, enhancing mass transport by several orders of magnitude compared to RDE [9]. Another approach is working with a gas diffusion electrode (GDE). While in RDE measurements the reactant mass transport is severely limited by the gas solubility of the reactant in the electrolyte, GDEs enable reactant transport rates similar to technical fuel cell devices, therefore the performance data obtained from GDE measurements can be directly compared to membrane electrode assembly (MEA) tests, but without the burden to set-up and manage the complete fuel cell device. Arenz and co-workers designed and proposed a GDE half-cell (A-GDE) device [10] where the catalysts are loaded on a gas diffusion layer, which is sandwiched between a gas holder and an ion exchange membrane. The latter separates the electrolytic solution, where the counter and reference electrodes are dipped in (Figure 1) [10]. This setup proved to be useful for the fast screening and testing of low-temperature PEMFC catalysts, obtaining similar results as in MEA measurements. In this paper A-GDE cell is used to mimic a proton exchange membrane fuel cell cathode for characterizing PGM-free catalysts and results are compared and discussed in comparison to the RRDE findings. Guiding papers have been published in recent years showing that GDE is a key tool for the investigation of the layer properties of ORR catalysts. Ehelebe et al., in a cross-laboratory experiment, show that for Pt-based catalysts important parameters to control are the iR and the homogeneity of the catalyst, especially when very small geometric surface area setups are used [11]. In the field of Pt-based material also Riasse et al. published a comparison between RDE and GDE, showing that under certain potential windows and experimental conditions, the GDE is a possible bridge between RDE and differential cell which resembles a fuel cell [12].

Another parameter that is often complicated to gouge is selectivity. While RRDE provides a rapid screening method for determining a material's tendency to reduce oxygen to either water or hydrogen peroxide, its accuracy can be influenced by the quality of layer deposition and loading. Trapping effects may occur, leading to a false four-electron reduction [1]. In this research work, the use of a GDE in a divided cell setup allows to evaluate the hourly production of hydrogen peroxide under operative conditions, namely during electrolysis at fixed potential or current. This also allows to evaluate the stability of the material since the variation of current in time is linked to durability. For this type of setup, several commercial, homemade, or customized cells are available, like the one from Gaskatel (G-GDE), which allows testing the material deposited on a gas diffusion layer with a high geometric area (3 cm^2) in divided or undivided cell configuration. The two different GDE set-ups also allow to perform accelerated stress tests (AST) to understand better the stability of the material and how this depends on its physical-chemical properties. This was also compared to stress tests done with RRDE to understand how the result obtained with different experimental conditions can match or diverge. The current literature shows that characterization made on different setups has been proposed mainly for Pt [10–14] and Fe-N-C in alkaline media only [2] or as a side characterization [15]. Hence, in this paper, we considered a benchmark Fe-N-C catalyst, that was characterized via RRDE, A-GDE cell, and G-GDE cell in acidic and alkaline media looking at the possible different effects in activity, selectivity, and stability also considering the variation of site density and turnover frequency of Fe-N_x active site.

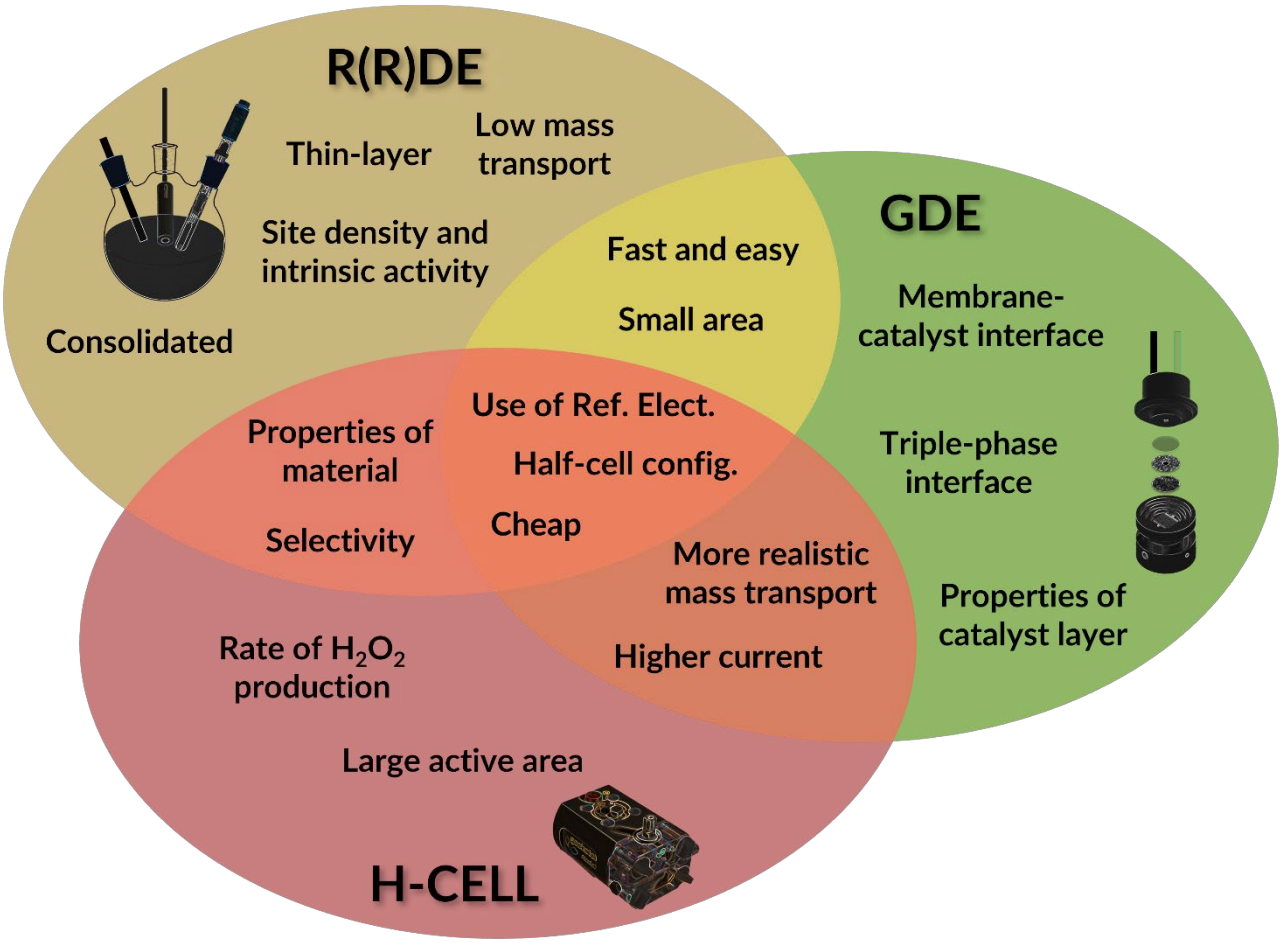

Figure 1. Scheme of the different electrochemical set-ups for gauging the Fe-N-C catalyst activity, selectivity, and stability.

2 Experimental

2.1. Chemicals

Sulphuric acid (93-98%, TraceSELECT, Honeywell Fluka), Potassium Hydroxide (86.4% assay, Sigma Aldrich), Nafion (5 wt.% in a mixture of lower aliphatic alcohols and water), Ethanol (HPLC grade > 99.8%), THF (HPLC grade > 99.9%), Acetone (HPLC grade > 99.9%), Acetic Acid (> 99.8%), Sodium Acetate trihydrate and Sodium Nitrite were purchased from Sigma-Aldrich and Carlo Erba reagents and used without any purification. Vulcan XC72 and 1,10-Phenanthroline (> 99%) were acquired from FuelCell store (USA) and Alfa-Aesar, respectively. Carbon paper (Toray

TP-120T-T20 and Sigracet 39BB) with PTFE treatment, Nafion 117, and FM-FAA-3-PK-75 were purchased from Hydro2Power SRL and used as received.

2.2. **Synthesis**

The benchmark catalyst (Fe2XC72) that was selected to perform all the measurements was synthesized according to previous work [16]. In brief, the synthesis consists of three steps (heat treatment/acid-leaching/heat treatment) with Vulcan XC72 as carbon support and $Fe(phen)_3Cl_2$ as Fe/N precursor (phen = 1,10-phenanthroline). The catalyst has 0.82 wt.% of nitrogen (elemental analysis - EA) and 0.34 wt.% of Fe (ICP-MC) which result in a Fe-N_x site density of 4.24 x 10^{18} sites g^{-1} (NO_2 stripping [17], see also further in the text and SI). XAS measurement confirmed the single-site nature of this catalyst with the absence or very low amount of nanoparticles (SI-S3) [15].

2.3. **Electrochemical tests**

2.3.1. Stripping for Site Density (SD) and turnover frequency (TOF) determination

Determination of the site density of Fe-N-C materials has been always a challenge, there are a lot of molecules that can interact with Fe-N_x center which are believed to be the main active sites. For example, HS^-, CN^-, or SCN^- have been used to poison the site, but a quantitative determination is not possible [18–20]. The two main methods that have been developed to obtain quantitative analysis are CO pulse chemisorption/desorption [21,22] and NO stripping [22–25]. The former is generally able to provide a more accurate determination as the probe molecule is smaller and easily reaches the metal site, but suffers from the experimental conditions and, unlike the latter method, is not an electrochemical determination. Indeed, NO stripping is performed under more similar conditions to R(R)DE analysis, and in principle, it gives a clearer idea of the electrochemically active sites. This anyhow suffers also of some drawbacks, first of all, the specificity of NO adsorption is not fully understood, for example, it has been shown that adsorption on FeO_x could occur [26], and functionalized nitrogen carbon material has a non-negligible response [15]. Furthermore, the

stripping analysis determination is restricted for analysis in acid electrolytes since in alkaline media the behavior of Fe-N_x-based catalysts is generally different [16]. A further aspect to take into account is that this method is time-consuming since a single determination requires up to 6/7 h of measurement (following the published and adapted procedure) and it is heavily influenced by the quality of the drop casted layer. Nevertheless, it remains one of the few methods, and perhaps the only electrochemical one, that allows a reliable estimation of Fe-N_x active sites.

The NO stripping technique requires a classical 3-electrode setup, where the electrolyte is an acetate buffer. The adoption of this media was in the idea of the proposer the most suitable compromise to mimic an acid measurement, but at the same time to have a sufficient potential window to observe the NO stripping without hydrogen evolution interference. LSVs are recorded in an oxygen-saturated solution before poisoning, after poisoning, and after stripping. The stripping procedure is a simple cyclic voltammetry (in oxygen-free solution) where a reductive peak appears because of the reduction of NO to ammonia, which makes the stripping charge linked to the amount of NO molecules and so to the number of Fe-N_x sites in the material according to the formula:

$$MSD\ [mol\ sites\ g^{-1}] = \frac{Q_{strip}[C\ g^{-1}]}{n_{strip}F[C\ mol^{-1}]} \quad (1)$$

where n_{strip} is the number of electrons associated with the reduction of one adsorbed nitrosyl per site to NH_3 (or more precisely to NH_4^+), which is equal to 5. The turnover frequency (TOF) of Fe-N_x sites is then given by the expression:

$$TOF[e^-\ sites^{-1}\ s^{-1}] = \frac{j_K\ [A\ g^{-1}]}{MSD[mol\ sites\ g^{-1}] \cdot F[C\ mol^{-1}]} \quad (2)$$

where F is the Faraday constant, j_k is the kinetic current (or mass activity) determined by the Tafel plot. Clearly, non-specific adsorption leads to a systematic error, that in any case was shown to be negligible in most of the cases [17]. A detailed procedure with all the steps is reported in Supporting Information (S1).

2.3.2. R(R)DE setup and method

For ORR investigation the RDE configuration is usually implemented with the addition of a probe (a Pt ring) to detect the possible hydrogen peroxide production, from the name Rotating Ring Disk Electrode. RRDE is, in theory, useful for all electrocatalytic reactions in which multiple products are possible, like H_2O_2 and H_2O for ORR or CO, H_2, CH_4, etc. in CO_2RR. In practice, the selectivity of ring material, which is generally Pt, made this device almost specific for O_2 reduction. Only recently a configuration with Au as a ring has been suggested for CO_2 reduction to detect CO, but the possible application for quantitative analysis is still to be proven [27,28]. Linear sweep voltammetries (LSVs) were carried out on an RRDE, Metrohm: ∅ = 5 mm GC disk and a Pt ring in both Ar-purged and O_2-saturated 0.5 M H_2SO_4 and 0.1 M KOH solution, using an Autolab model 101N potentiostat or a PARSTAT 3000A-DX. Other pH values were tested starting from a 0.1 M phosphate buffer and adjusting the pH by the addition of small quantities of an acid (H_2SO_4) or alkaline (KOH) solution until reaching the desired pH value. All the measurements were done in a three-electrode cell thermostated at 25 °C. The RRDE tip was used as a working electrode, a graphite rod was used as counter-electrode, and, for acidic electrolyte, a homemade RHE as a reference electrode was prepared before each experiment according to a literature procedure [29]. For intermediate pH, an SCE saturated electrode was used, while for the measurements in KOH, a Hg/HgO (AMEL instruments for Electrochemistry) reference electrode (E_{RHE} = 0.098V + 0.059pH + $E^0_{Hg/HgO}$) was adopted. The calibration of the Hg/HgO reference electrode was performed in a standard three-electrode system where two polished Pt wires were the working and counter electrodes, respectively and the Hg/HgO electrode was the reference electrode (see Supporting Information of reference [16])

The number of transferred electrons (n) was determined by RRDE linear sweep voltammetry (2 mV s^{-1}) according to the following equation:

$$n = \frac{4|i_D|}{|i_D|+|i_R|/\mathrm{N}} \quad (3)$$

Where i_D is the current recorded at the disk, i_R is the current recorded at the ring, and N is the collection efficiency, which is equal to 0.25 (determined by considering the monoelectronic reduction of

$K_3Fe(CN)_6$ standard), the ring potential was set to 1.5 V vs. RHE. With the last analysis, it is also possible to evaluate the percentage of hydrogen peroxide (eq. 4) produced at the working electrode by rearranging eq. 3 :

$$\%_{H_2O_2} = \frac{100(4-n)}{2} = \frac{100 \cdot 2|i_R|}{N \cdot |i_D| + |i_R|} \quad (4)$$

Accelerated stress tests were performed on RDE employing intensive cycling (7000) between 0.55 and 1.05 V as reported in the literature [30]. This test is a variation of stress tests for Pt/C fuel cell catalysts reported by Ohma et al. [31] which is generally conducted between 1.5 and 1.0 V and extended also to M−N−C [32,33]. In other words, a triangular wave was applied to the potential region 0.55-1.05 V instead of a square one [33–35]. The measurements were performed in the O_2-saturated electrolyte (0.5 M H_2SO_4 or 0.1 M KOH) at a scan rate of 200 mV s^{-1}. The activity was checked by performing LSV at 5 mV s^{-1}.

2.3.3. GDE setup and method

The A-GDE cell is commercially available (gde-cell.com) and sold as a steel body that serves also as a contact for applying the potential to the working electrode, which consists of a catalyst-coated carbon paper [10]. The same is also possible with a PEEK body with metal contact as proposed in other work [36] and as used in this paper. Therefore the contract is guaranteed by a small stainless steel rod under the carbon paper layer. The latter cell was crafted in our laboratories. Contrary to the original setup a carbon felt under the carbon paper was used to improve the electrical contact between the electrode and the cell body since it does not interfere with the electrochemical measurement. This could become unavoidable because carbon paper and Nafion membrane are sold with different thicknesses and a constraining thickness is necessary to obtain good contact between the catalyst and membrane. As anticipated, a Nafion membrane (Nafion 117, QuinTech) was placed between the catalyst and the upper body (made of Teflon) of the cell. The very same configuration but in alkaline media with a suitable anion conductive membrane (FM-FAA-3-PK-75, QuinTech) is proposed and tested here [37,38]. The results obtained are superimposable using the two membranes in alkaline pH

(Figure S7). The carbon paper/membrane sandwich guarantee that no electrolyte passes through the cell, so corrosion is not a relevant issue in this set-up, also having almost the entire body in PEEK is an advantage. A graphite rod was used as a counter electrode and an RHE, SCE, or Hg/HgO for acid electrolyte, intermediate or alkaline media respectively, as reference electrodes. The scheme is depicted in Figure 2. The setup is easy to prepare; the membrane is clamped on the carbon paper and the pressure is sufficient to induce a good adherence. In such a configuration and using 0.5 M H_2SO_4 as electrolyte a cell resistance of 20 Ω is measured. When the current flow is too high to perform accurate ohmic drop compensation, an acid concentration higher than 0.5 M may be required. For example, Arenz and co-workers use 4 M $HClO_4$ to reduce ohmic drop but this was not the case with Fe-N-C materials.

Cyclic voltammetry and impedance spectroscopy under Ar or O_2 flux were used to characterize the electrochemical behavior of the material, while chronoamperometry or chronopotentiometry was performed to verify the material stability/durability. Also, impedance spectroscopy analysis can be carried out to evaluate the ohmic drop. More in detail ASTs were performed using intensive cycling, as done for RRDE and chronoamperometry at 0.2 V vs. RHE (at pH 0.3 and 14) and 0.6 V (pH 0.3). Before and after AST, the activity was tested for each trial. Activity loss is evaluated as onset potential (E at 2 mA cm^{-2}) variation and percentage of current variation at a certain potential.

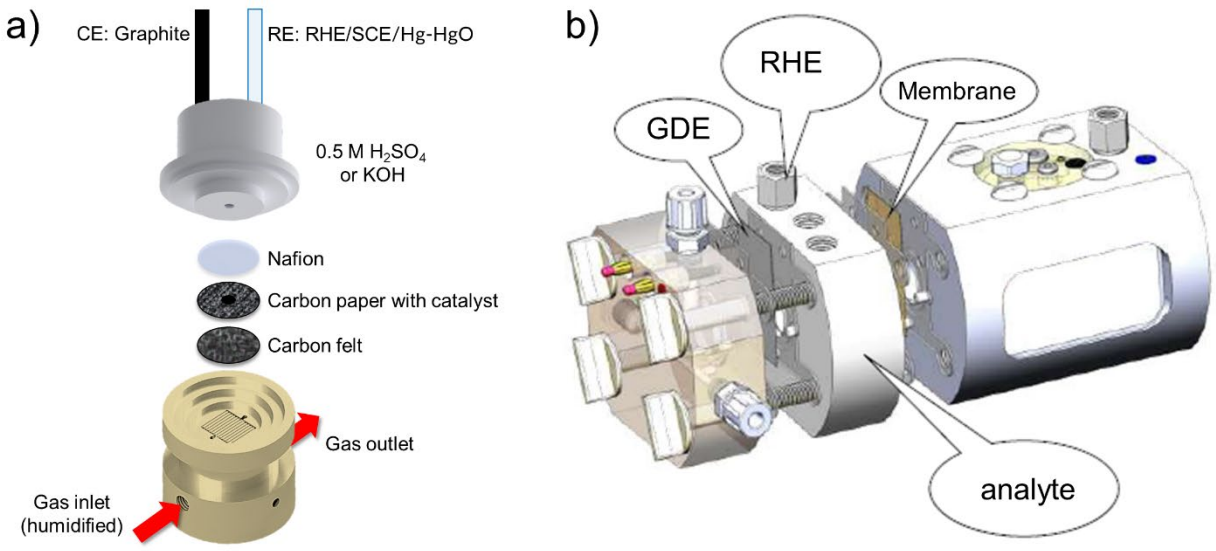

Figure 2. a) Scheme of the A-GDE cell in all its components; b) Scheme of the G-GDE cell for electrolysis; the component in the middle is the additional chamber to perform measurements in a divided cell.

2.3.4. Electrolysis setup and method

The electrolysis measurements were performed with a commercial cell from Gaskatel GmbH (G-GDE cell, Figure 2b). It consists of a primary cell and a gas feed chamber made of polypropylene (PP), which allows it to feed the gas from behind the GDE, which faces the electrolytic solution. An optional secondary compartment could be inserted in between the two main components to perform electrolysis in a divided chamber configuration (Figure 2b). In this latter case, the cation/anion conductive membrane allows separating the two chambers allowing the quantification of electrolysis products. In this configuration the working electrode is the gas diffusion electrode, the counter electrode is a Pt wire, and the reference electrode is a RHE supported in a Lugging capillary.

ASTs were performed using chronoamperometry at 0.2 V vs. RHE (at pH 0.3) and 0.6 V (pH 0.3 and pH 14). Before and after AST, the activity was tested for each trial. Activity loss is evaluated as onset potential (E at 2 mA cm^{-2}) variation and percentage of current variation at a certain potential. A sampling of the solution was done for H_2O_2 quantification and to evaluate the faradic efficiency. The

quantity of H_2O_2 produced was assessed using a spectrophotometric technique (see supporting information S1.2) that involves the reaction of the peroxide with potassium titanium oxide sulfate to form a complex, which has a maximum of absorption at 410 nm (Figure S1 and S2).

3 Result and Discussion

Fe2XC72 catalyst was synthesized by thermal treatment of Tris-1,10-phenanthroline iron(II) chloride and Vulcan XC72. The chemical composition was analyzed using elemental analysis, which revealed carbon and nitrogen contents of 90.60% and 0.82%, respectively. The iron content (0.34%) was determined using ICP-MC. In a previous paper, HR-TEM and XAS measurements performed at the Fe K-edge confirm the presence of Fe-N_4 active sites in the samples (Figure S3) [15]. The results showed that the Fe atoms were dispersed on the carbon matrix, with the Fourier transform of the EXAFS signal exhibiting a first peak at around 1.5 Å and a minor peak at 2.6 Å. These peaks were assigned to the Fe-N first coordination shell and Fe-C backscattering from the second coordination shell, respectively. The EXAFS spectra were fitted assuming the presence of in-plane nitrogen atoms and oxygen atoms as axial ligands. The analysis revealed that the Fe-N coordination number was around 4, indicating that iron forms Fe-N_4 moieties. Finally, the absence of Fe-Fe backscattering confirmed the absence of metal NPs.

3.1. Electrochemical performances: Loading Effect

Testing a catalyst in a half-cell configuration can be challenging because several variables could affect the recorded activity, potentially leading to an unrealistic estimation of the catalyst's performance. The two main examples are the good dispersion of a catalyst powder on the R(R)DE surface and the strength of binding that is needed to prevent detachment from its surface. This, in general, forces modification of the catalyst loading, which might impact the result of a measurement, for complex reactions such as CO_2RR and ORR. In 2008 Dahn & Co. pointed out the importance of

the correlation between loading and hydrogen peroxide production since, in particular in mild acidic electrolytes, passing from 800 µg cm^{-2} to 80 µg cm^{-2} results in an increment of H_2O_2 production from 10% to 70% at around 0.6 V vs. RHE [39]. If a 2-electron pathway is more prevalent than a 4-electron pathway or a highly efficient 2x2 electron pathway, the selectivity towards hydrogen peroxide could be distorted when a thick layer is used. This is because if H_2O_2 becomes trapped within the catalyst layer, it can be further reduced, resulting in an overestimation of catalyst selectivity. This effect is also linked to the pore network of the material and different results can be observed for different pore size distributions in the catalysts. For that reason, the effect of loading was compared at both R(R)DE and GDE set-up, focusing on both activity and selectivity for the former, and on activity for the latter. A last effect could be caused by the real electrochemically active area which change by changing the loading. This effect primarily impacts the limiting current in RRDE, which cannot easily help in determining the number of transferred electrons during the reaction. This is why RRDE is preferred to KL from RDE to estimate the selectivity.

3.1.1. R(R)DE

The RRDE loading effect of benchmark catalyst Fe2XC72 is shown in Figure 3, loading from 0 (naked GC) to 0.8 mg cm^{-2} were tested. Figure 3a reports the LSV at different loadings normalized by the geometric surface area. It is clear that the limiting current decreases by decreasing the loading on the GC surface, but the gravimetric limiting current scales inversely (Figure 3b). In addition, from 0.4 mg cm^{-2}, the curve shape starts to stabilize, namely a steady value of limiting current is approached. Also, the half-wave potential is affected by the catalysts loading, varying from 0.375 to 0.752 V vs RHE (Figure 3c). In 0.5 M H_2SO_4 even at a loading of 0.025 and 0.050 mg cm^{-2} the amount of peroxide is low (< 10%) as suggested by Figure 3d, meaning that this catalyst in acidic electrolyte tends to produce water rather than peroxide, i.e., almost 4 electrons are exchanged. Even if the lower amount of catalyst results in a lower current density (Figure 3e), the kinetic current (or current normalize by the loading) appears to be not affected by the amount of catalyst, actually it

results even higher at low loading (Figure 3b,f). So, it can be argued that current density, normalized for the geometric area, is certainly not a reliable parameter. On the other hand, determining the electrochemically active area for metal-free or nearly metal-free materials is not a straightforward task and can be prone to errors. This is because the only viable method involves determining the capacitive component of the current from cyclic voltammetry measurements [40]. This aspect is important for a better understating of real material activity since focusing on a single loading could lead to a partial understanding of a certain material. Further insights and comments on such behavior will become available by H_2O_2 quantification as reported later in the text.

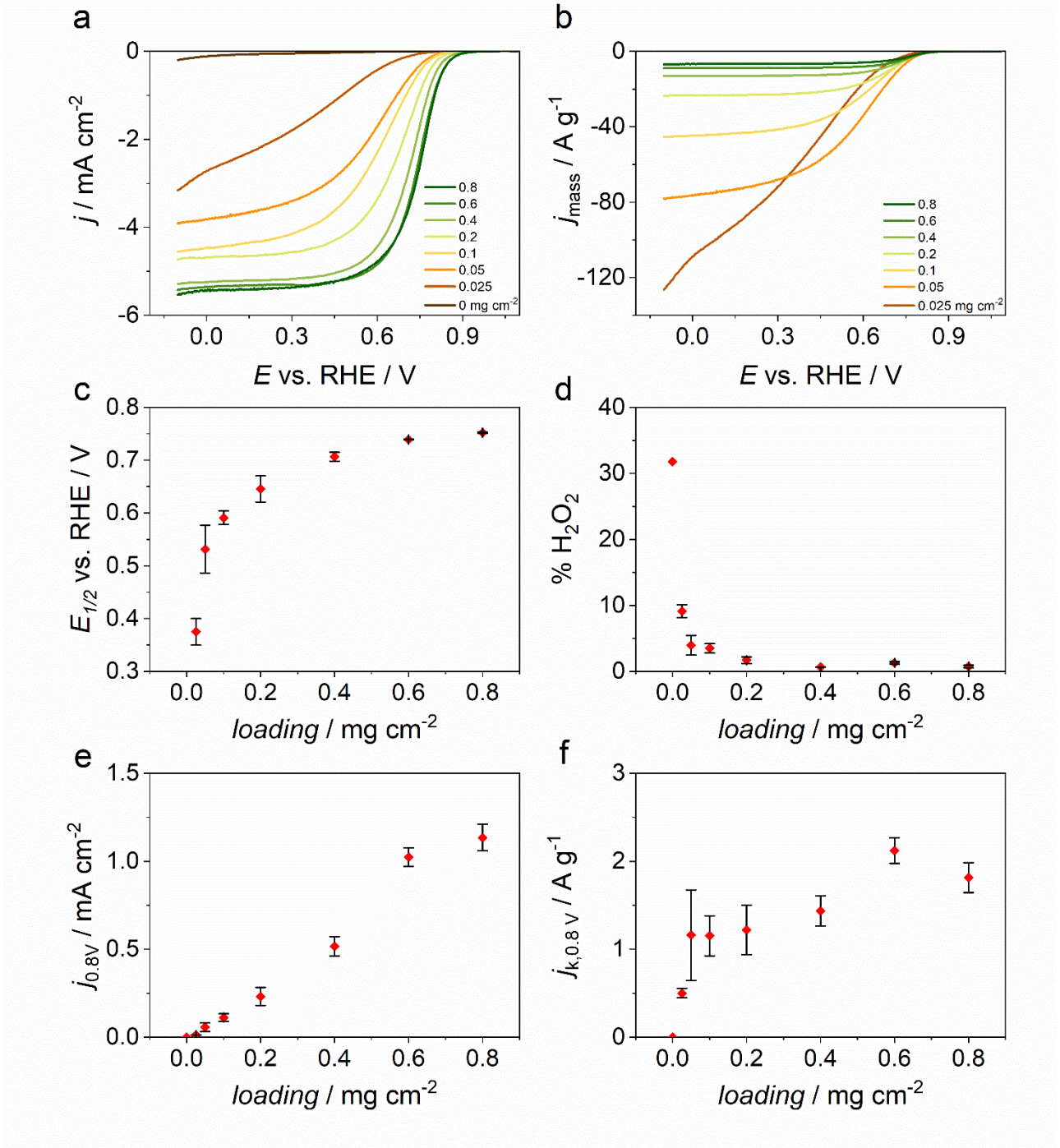

Figure 3. Electrochemical data from LSV at RRDE (2 mV s^{-1}, 1600 rpm) of Fe2XC72 recorded in O_2 saturated 0.5 M H_2SO_4 a) LSVs normalized by the geometric area, b) LSV normalized by the loadings. c) Half-wave potential and d) peroxide yield as a function of different loadings. e) current density at 0.8 V vs. RHE and f) kinetic current at 0.8 V vs. RHE at 8 selected loadings.

3.1.2. A-GDE and G-GDE

The loading effect was also evaluated with a gas diffusion electrode cell. In this setup, the catalyst is no longer in direct contact with the electrolyte solution, which serves only as a proton source (in the case of ORR), while the gas flows from underneath the carbon paper and through it until reaching the catalysts layer deposited on its upper surface. Eight different loadings were prepared ranging from 0 (sole carbon paper) to 4.0 mg cm^{-2}. It is possible to observe that even at low loading there is a huge increment in activity compared to the sole carbon paper (Figure 4a). The increasing effect of the loading fades after reaching a value of 0.5 mg cm^{-2} (Figure 4a), but the current increment is still detectable till reaching a loading limit after 3 mg cm^{-2}. The choice of higher loading, compare to RRDE, is done since generally under GDE setup a higher loading is used [2,11]. Looking at the normalized current values (Figure 4b,d) it is possible to observe that the activity per mass unit increases with the decrease of the loading, which is in agreement with what has already been observed at RRDE (Figure 3). This effect is explanatory of the fact that an increase in loading only leads to an increase in electrode thickness but not in active surface area (active material). This becomes particularly noticeable when considering higher loadings, where an increase of 0.2 mg cm^{-2} does not result in a change in activity, but instead leads to a kinetic current value that remains substantially constant (Figure 4d). So, in conclusion, higher loading allows us to obtain a higher current, but in terms of mass-corrected current, the optimal loading is between 0.5-1.0 mg cm^{-2}.

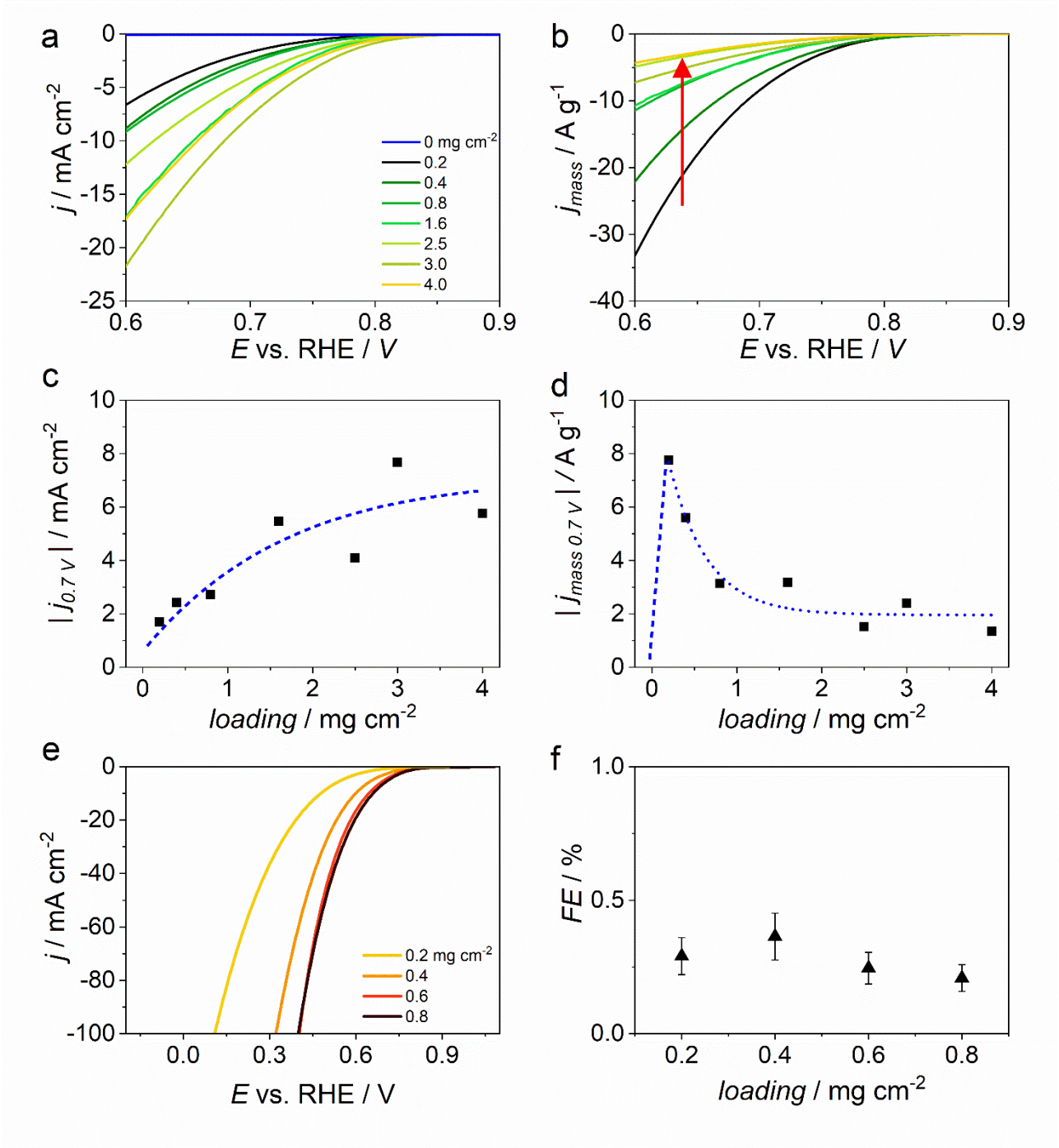

Figure 4. a) LSV recorded at A-GDE at different loadings (only cathodic scan is reported for clarity) on carbon paper where loading 0 is the sole carbon paper (0.5 M H_2SO_4, O_2 flux 100 mL min^{-1}), b) current normalized for the carbon loading, c) Current density (surface area normalized) and d) specific current density (catalyst mass normalized) determined at 0.7 V vs. RHE at different loadings, e) ORR response at different loading in G-GDE cell configuration and f) faradic efficiency after 7 h at 0.2 V vs. RHE respect to the loading.

The loading effect was also tested on the divided G-GDE cell set-up, where the GDE electrode was prepared precisely as in the A-GDE cell, using the drop casting method. However, this resulted in a dataset that was not comparable to either RRDE or A-GDE results. Therefore the GDE electrode was prepared by optimizing the casting procedure till reaching comparable results between the two GDE setup (refer to the casting method and ink composition in the SI for more details). The expected outcome was observed as the current increased with higher loadings till reaching a superimposable behaviour (refer to Figure 4e). Furthermore, a stable Faradaic efficiency (FE) for H_2O_2 of approximately 0.3% was achieved (refer to Figure 4f). We limited our analysis to 0.8 mg cm^{-2} since in the absence of a membrane on top of the catalysts the layer became thick and less stable. It is to emphasize that in the non-optimized layer, a decrease in current was observed with increasing loading, which was observed during attempts to improve the ink composition and catalyst casting on the carbon paper support (Figure S4). This phenomenon was attributed to an increase in the hydrophobicity of the casted material, wherein a thicker layer could lead to reduced surface wettability and subsequently lower site utilization. This deduction is supported by contact angle analysis, which revealed variations in contact angle corresponding to the catalyst loading. (Figure S4).

3.1.3. NO Stripping

The NO stripping method allows to electrochemically probe the number of Fe-N_4 sites, even if the method underestimates the true density of the active site. In Figure 5 the key measurement results are reported. The NO stripping charge is obtained by the difference of the responses of the poisoned and unpoisoned catalyst layers (Figures 5a and b), which allows calculating the SD (eq. 3), while the variation of current recorded at a given potential (Figure 5c and d) could be used to evaluate the TOF at that potential (eq. 4) since the overall activity at a certain potential is proportional to the product of TOF and SD.

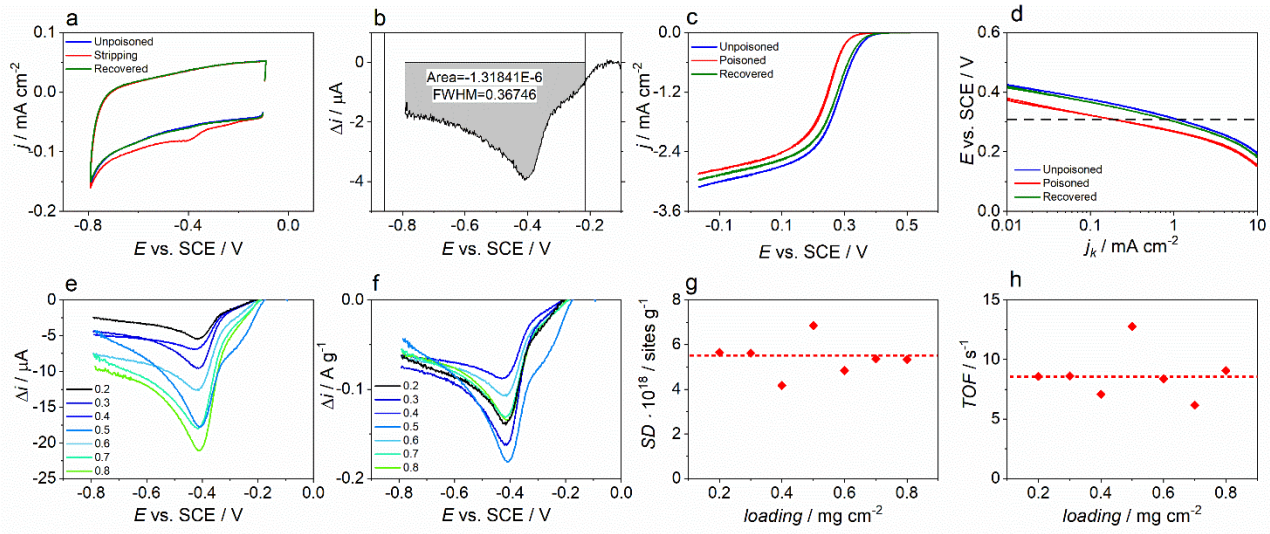

Figure 5. Voltametric response during a typical stripping analysis recorded in acetate buffer: a) CV in the stripping region before, during, and after stripping in argon purged electrolyte, b) stripping charge area extrapolated from the CV showed in 'a', c) LSV at 1600 rpm, d) Tafel plot in O_2 saturated electrolyte, e) Stripping peak derived from subtraction of stripping CV and background, f) the same peak normalized for the loading on the electrode, g) SD and h) TOF vs. the loading on the electrode.

Stripping measurements are performed on catalyst layers with varying loadings to evaluate the effect of loading on-site density determination. The SD is a specific gravimetric value, therefore its value is not supposed to depend on the catalyst mass, even if at very high loadings a dependence is not to be excluded, because of an overestimation of the real active mass. In the present case loadings in the range 0.2 to 0.8 mg cm^{-2} were considered (Figure 5e,f), and as reported in Figure 5g SD data are slightly scattered around an average value. We conclude that there is not, as expected, a dependence from the loading, which also allows us to state that the site per unit area is almost constant in this range of loadings. This is a confirmation of the validity of the method in a wide range of loadings, that, up to our knowledge, it was never evaluated in literature. Therefore, it is possible to define an SD number as the average value associated with an error calculated with half-dispersion or by standard deviation. The same is true for the TOF (Figure 5h). What is evident is that the error associated with the method, in terms of standard deviation, spans from 10 to 20% for SD and TOF.

This also suggests that being stripping a delicate measurement, at least 3 different independent determinations should be carried out.

3.2. Effect of pH at R(R)DE and GDE

It is well known that pH has an impact on the activity, durability, and selectivity of Fe-N-C materials. Typically, this can be easily confirmed by employing 0.5 M H_2SO_4 and 0.1 M KOH as electrolytes during R(R)DE analysis. However, in this study, we have also included intermediate pH values obtained using 0.1 M phosphate buffer that was adjusted to the desired pH. Nitrogen-doped carbon material activity recorded in alkaline media is higher than in acidic conditions (Figure 6a). Indeed, the active sites of oxygen reduction are different passing from one electrolyte to the other one and it seems that the role of the metal is less important, since also materials that show poor performance in acid conditions perform well when passing to an alkaline solution [16]. For that reason, metal-free catalysts are generally more attractive to be used in alkaline conditions if not meant to produce hydrogen peroxide, which is less stable under high pH. The different activity, which is linked to different active sites, leads generally to different peroxide production for example Fe2XC72 shows a yield of peroxide lower than 1% in acid and close to 5% or even higher at pH 12 (Figure 6b). The half-wave potential ($E_{1/2}$) increases linearly from pH = 3 to pH = 13, with a slope of 36.1 ± 3.0 mV/pH, (Figure 6c). By looking at the whole set of pH there the trend appears as a reverse volcano plot with a minimum at pH 3, which coincides with the worst activity. This behavior was somehow observed also by Rojas-Carbonell et al. [41] even if with much more scattered points. As reported in several papers the rate-limiting step in very acidic media does not depend on pH or the concentration of H^+. On the contrary, in weakly acidic to alkaline electrolytes the rate-limiting step is dependent on the hydroxyl concentration and a slope of approximately 30 mV/pH indicates that the first electron transfer step is rate-limiting [42].

The effect of pH on the H_2O_2 selectivity is reported in Figure 6d at two different potentials. At both potentials (E = 0.6 V and E = 0.3 vs RHE), the H_2O_2 yield is almost constant, with values

fluctuating around 1%, in the pH range 0-14, with an apparent increase of the yield at higher overpotential at alkaline pH. The potential 0.3 was purposely chosen since a more appreciable difference is observed between various pH aven if 0.6 V vs SHE is clearly 0.6 more of interest for fuel cells. Another point to remark is that the limiting current around 4/5 mA cm^{-2} is lower than the theoretical for a four-electron transfer even though the amount of hydrogen peroxide is very low. This is very often observed for these materials [35] and we retain it is related to the casting procedure and to the real surface area which is different from the geometric one. In fact it could for sure be also an effect of selectivity, but it seems to not match with what was observed in RRDE and G-GDE where the selectivity remains low even at low loading (Figure 3a,d and Figure 4f).

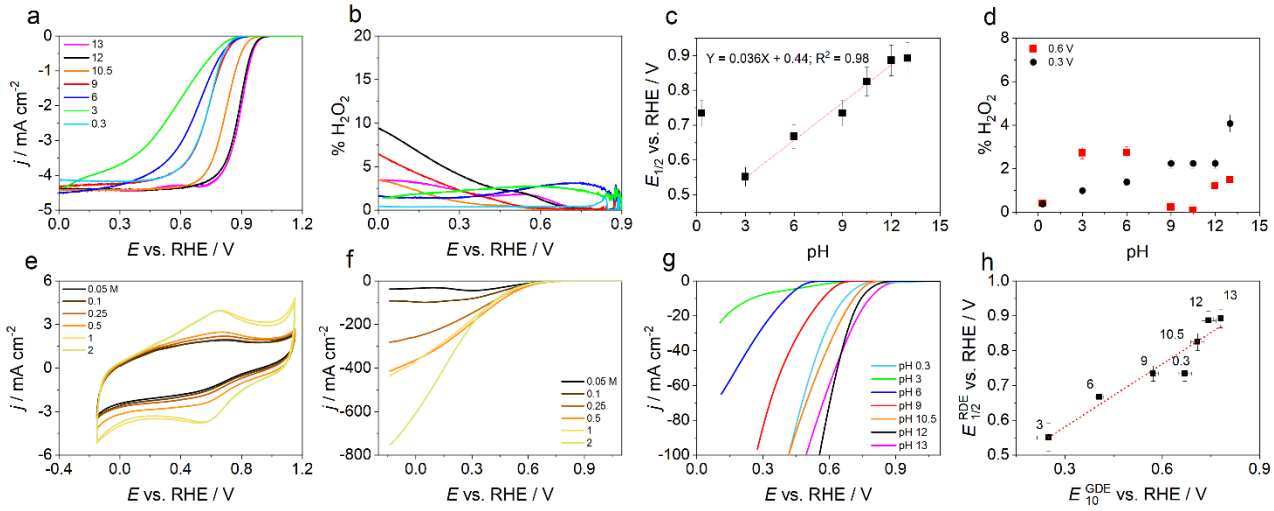

Figure 6. a) LSVs of Fe2XC72 recorded at different pH at RRDE (2 mV s^{-1}, 1600 rpm), b) yield of hydrogen peroxide, c) variation of half-wave potential as a function of pH, d) H_2O_2 yield variation as a function of pH, e) Cyclic voltammetry under Ar flux, f) voltammetric response (cathodic run) at a different acid concentration under oxygen flux at the different molarity of sulphuric acid in the upper part of the cell, g) Response at different pH and h) correlation between RDE and GDE test in terms of half-wave potential and onset (E_{10}, at 10 mA cm^{-2}) respectively.

In the A-GDE cell, changing the pH means changing the proton concentration in the upper part of the cell containing the electrolyte, namely above the Nafion membrane. This, in turn, should result in a different proton availability at the catalyst-membrane interface and therefore an impact on the

activity and selectivity is to be expected. Figure 6e shows the different voltammetric responses at the A-GDE electrode, of Fe2XC72, at different H_2SO_4 concentrations under a flux of argon. At first glance the effect of a different [H^+] is an increase of the capacity current and of the quinone-hydroquinone couple redox response (Figure 6e) [43,44]. In Figure 6f it is reported the response of oxygen reduction at the GDE electrode. It is possible to observe that at low H^+ concentration, the current responsible for the HER reaches a limiting value while increasing the H^+ concentration the expected curve increases without being limited at least for the investigated overpotentials. The onset potential is not affected by the H^+ concentration, while a clear effect of acid concentration is present at a more negative potential. Figure 6g shows the response at different pH, with the same electrolyte used for RRDE investigation (Figure 6a). For all experiments a Nafion membrane was used. For sake of comparison an alkaline membrane was as well adopted at pH = 13. Both Nafion and alkaline membrane show superimposable behaviour as reported in Figure S5. It is worth emphasizing that, even in the GDE setup, activity improves when passing to a more alkaline electrolyte, with a distinct minimum activity point observed around pH 3, as previously noted. If we now directly compare the results obtained from RRDE and A-GDE measurements in the different pH values, it is clear that there is a complete agreement between the two sets of results, which implies a clear and absolute interchangeability of the two techniques Figure 6h. In Figure 6h the $E_{1/2}$ at RRDE is plotted versus E_{10}, potential at GDE when a current of 10 mA cm^{-2} is flowing. The two parameters are associated with different potential regions; however, they serve as two independent activity descriptors. Furthermore, when utilizing parameters such as the potential at 0.5 mA cm^{-2} (for RRDE), which is approximately in the "onset" region of the curve (similar to E_{10}), the correlation yields consistent outcomes as well as for $E_{1/2}$. Therefore, notwithstanding the adoption of $E_{1/2}$ or of an onset potential the correlation holds attesting the complete superimposition of the two techniques.

3.3. Stability and durability tests comparison at R(R)DE and GDE setup

The RRDE set-up is widely employed for testing the catalyst stability in accelerated stress tests. In the present work, the AST at RRDE consists of 7000 cycles between 0.55 and 1.05 V vs. RHE. Two different conditions: pH = 0.3 (0.5 M H_2SO_4) and pH=13 (0.1 M KOH) were tested and results are reported in Figure 7a. It is evident that for the investigated material both the activity and stability are higher in an alkaline environment than for the acidic one (Figure 7a). By considering the shift of the half-wave potential ($\Delta E_{1/2}$) as a parameter for the loss of activity, $E_{1/2}$ moves 56 mV to more negative potential when the accelerated stress test is performed in an acidic electrolyte and only 3 mV in an alkaline one (Table 1). NO stripping analysis test was performed before and after AST through RRDE to evaluate any possible changes related to the modification or loss of Fe-N_x active sites. When tested in an acidic electrolyte, it was observed that although the intrinsic activity of the sites remained similar (TOF), the SD decreased. This suggests that some of the active sites were leached out under acidic conditions, and the residual activity can be attributed to the remaining, more stable sites. When the same test is performed in KOH electrolyte no significant change in activity and site density was observed, meaning that sites are more stable in this environment (Figure 7b) . A decrease in TOF was instead observed which is unexpected in light of the slight decrease in activity. However, it is worth stressing that Fe-N_4 is not the sole active site and its activity role in alkaline electrolytes might not be fundamental [15]. As a comparison, the same ASTs was extended to A-GDE cell (Figure S6a) showing, in this case, a very good stability. This could imply that subjecting the electrode material to repeated cycles on a A-GDE cell may not be an effective method of stressing it, or that the specific cell configuration provides preservation of the catalyst, because of the presence of the Nafion membrane stucked on it. To verify this, another AST was performed on the A-GDE cell. The test consists of a chronoamperometry performed at 0.2 V or 0.6 V vs. RHE for 8 h under oxygen flow (Figure 7c). The current recorded at 0.2 V vs. RHE in acid media (Figure 7c) averages around 85 mA cm^{-2} and gradually decreases over time. It was necessary to remove some bubbles formed at the counter electrode that tend to deposit on the lower part of the cell, creating resistance and a false current loss. LSVs were also recorded before and after the AST and are reported in Figure 7d and

Figure S6b,c. The stress effect appears very clear, as an example for the chronoamperometry at 0.2, the potential read at a current of 2 mA cm^{-2} shifts from 0.720 to 0.669 V, i.e. 51 mV. To compare the RRDE and A-GDE tests, a similar potential of 0.6 V vs RHE was considered. The current output at 0.6 V vs RHE before the AST was 9.01 mA cm^{-2}, but it dropped to 4.21 mA cm^{-2} after 8 hours, indicating an almost halving of the initial activity. The potential read at a current of 2 mA cm^{-2} shifts of 51 mV, a value that is in line with the one observed with AST at 0.2 V vs RHE. All these parameters show that the activity is lowered in good accordance with the AST performed on RRDE even if in the present case a chronoamperometry is necessary as a more stressful action, see for comparison data reported in Table 1. Chronoamperometry at 0.2 V vs RHE on A-GDE cell at alkaline electrolyte was also performed and it can be observed that again the alkaline media is more stable than the acidic one (Table 1, entry 6). It is noteworthy that measurements recorded under this setup are not straightforward due to the very high currents recorded, regardless of the type of membrane tested (Figure S5), and compensating for resistance proves to be challenging, in the sense that at high current compensation with lab-instrument became challenging and generally a post-run iR compensation need to be done by reconstructing the curve point by point with iR compensation in the aftermath [11]. In addition, it was observed that the electrode wettability increases by moving to alkaline pH (see contact angle measurements, Figure S7), and in any case varies over time, which results in a lowering of iR-drop as observed during the stress test. Consequently, there is the possibility of incorrect electrode evaluation during the test, which could potentially lead to counterintuitive results. In fact as the acid ORR produces water while the alkaline ORR consumes water, it is more intuitive that the electrode flood ad acid pH rather than at alkaline one, conversely to what observed here [2].

Table 1. Electrochemical parameters derived from accelerated stability tests of Fe_2XC72 electrocatalysts at RRDE, A-GDE cell in acid or alkaline electrolytes.

RRDE		$E_{j=0.1}$ V	$\Delta E_{j=0.1}$ mV	$E_{1/2}$ V	$\Delta E_{1/2}$ mV	$j_{0.6\ V}$ mA cm^{-2}	$\Delta j_{0.6}$ %
1	Before AST	0.853	-	0.681	-	2.89	-

	0.5 M H_2SO_4	after 7000 cycles	0.830	−23	0.625	−56	2.34	−19
2	0.1M KOH	Before AST	0.961	-	0.813	-	4.66	-
		after 7000 cycles	0.959	−2	0.810	−3	4.24	−9

	A-GDE cell		$E_{j=2}$ V	$\Delta E_{j=2}$ mV	$j_{0.6\ V}$ mA cm^{-2}	$j_{0.2\ V}$ mA cm^{-2}	$\Delta j_{0.6}$ %	$\Delta j_{0.2}$ %
3	0.5 M H_2SO_4	Before AST	0.785	-	20.02	243.29	-	-
		after 7000 cycles	0.776	−9	15.22	230.03	−24	−5
4	0.5 M H_2SO_4	Before AST	0.720	-	13.09	36.52	-	-
		after 8h at 0.2 V	0.669	−51	5.52	18.27	−58	−20
5	0.5 M H_2SO_4	Before AST	0.693	-	9.01	139.97	-	-
		after 8h at 0.6 V	0.638	−55	4.21	127.05	−53	−9
6	1M KOH	Before AST	0.857	-	64.27	236.20	-	-
		after 8h at 0.2 V	0.855	−2	46.75	236.66	−27	−10

	G-GDE cell		$E_{j=2}$ V	$\Delta E_{j=2}$ mV	$j_{0.6\ V}$ mA cm^{-2}	$j_{0.2\ V}$ mA cm^{-2}	$\Delta j_{0.6}$ %	$\Delta j_{0.2}$ %
7	0.5 M H_2SO_4	Before AST	0.728	-	12.57	458.7	-	-
		after 8h at 0.6 V	0.697	−31	6.43	167.4	−49	−64
8	0.5 M H_2SO_4	Before AST	0.712	-	9.45	351.4	-	-
		after 8h at 0.2 V	0.670	−42	4.05	162.0	−57	−54

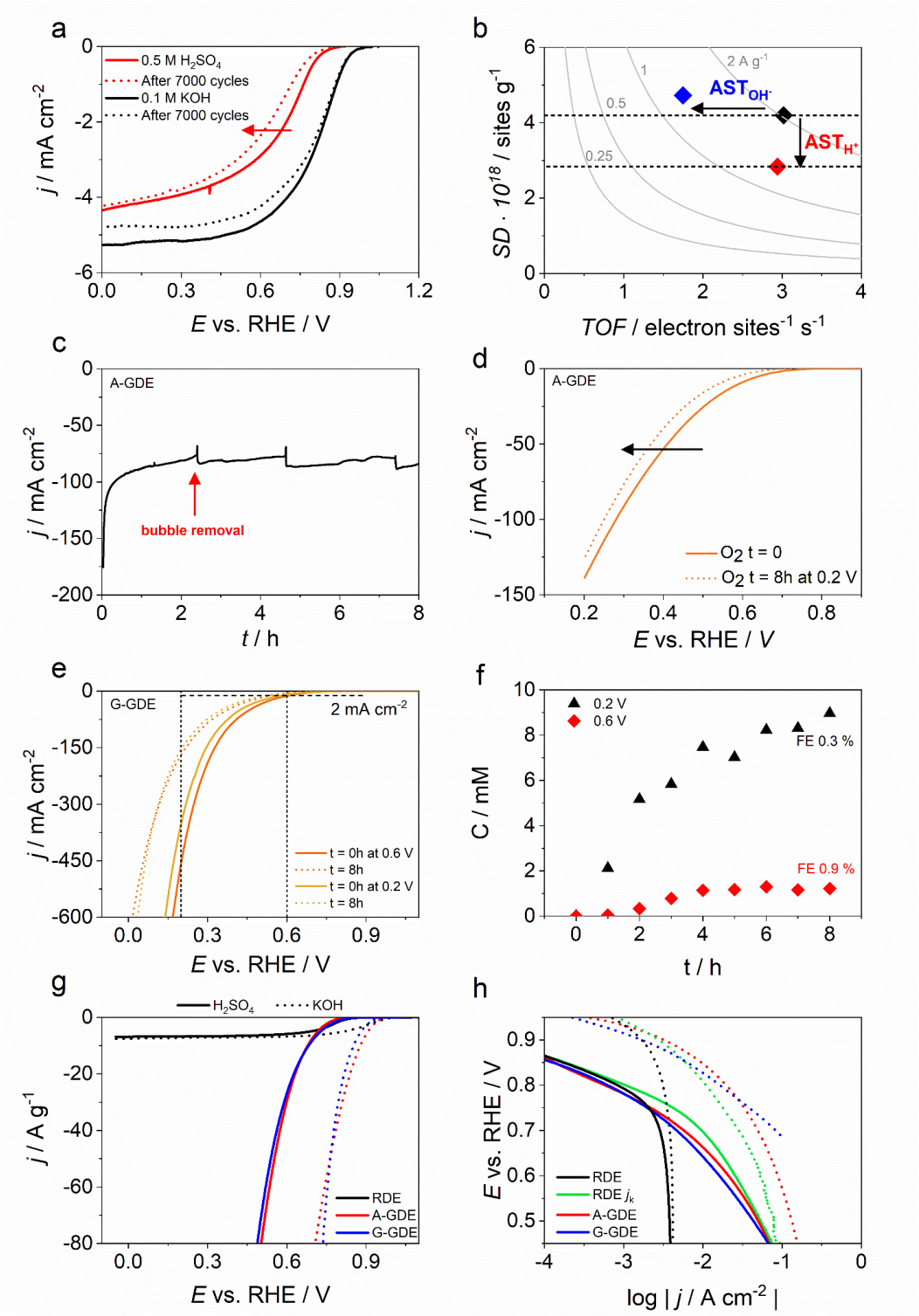

Figure 7. a) LSV evolution during AST recorded at RRDE in acid and alkaline electrolytes; b) variation of SD/TOF in acidic and alkaline electrolytes, after the AST, reported in an iso-current map; c) chronoamperometry test at 0.2 V performed at A-GDE half-cell in H_2SO_4 electrolyte under O_2 flow, d) CV shift recorded at A-GDE electrode in acid electrolyte after the 8 h of AST (curves are background subtracted), e) LSV at G-GDE cell before and after chronoamperometry at 0.6 and 0.2 V

vs RHE (AST) in acid media and f) peroxide concentration determined by titration method using Ti (IV), the final FE is reported, g) RDE vs. A-GDE vs. G-GDE cell the scale is the current density normalized by loading in acidic and alkaline electrolytes, h) Tafel plots for the three different setups with RDE kinetic current correction for both electroyltes.

The hydrogen peroxide yield is often calculated via RRDE analysis (equation 4) or sometimes with the less accurate Koutecky-Levich plot by RDE analysis at different rotation speeds. A-GDE cell setup previously described is close to a real fuel cell setup but does not allow the quantification of hydrogen peroxide production so a direct comparison in terms of selectivity between the two techniques cannot be made. The G-GDE divided cell (Figure 2), mounting a large surface area GDE electrode, allows us to quantitatively evaluate the H_2O_2 yield, and the faradaic efficiency and therefore to have a more accurate evaluation of the number of transferred electrons and mechanism. This setup is certainly more useful for electrolytic *in situ* production of H_2O_2 but it could confirm how catalysts for fuel cells perform under different conditions compared to RRDE, but without the concern about ancillary components and controls present in a fuel cell. More practically, the catalyst was put on a carbon paper with a loading of around 0.6 mg cm^{-2} on an area of 3 cm^2 which is the active area under this setup. The electrolyte was, as for RRDE experiments, 0.5 M H_2SO_4 and LSVs were recorded before and after 8 h of chronoamperometry at 0.2 V or 0.6 V vs. RHE. This experiment serves also as AST (Figure 7e). It is noticeable that the two distinct current profiles, pre- and post-AST, demonstrate a decline in performance and, consequently, a reduction in catalyst activity. As an example, considering an onset current of 2 mA cm^{-2}, there is a shift of potential ($\Delta E_{j=2}$) of 42 mV, which is in line with what is observed for the $\Delta E_{1/2}$ shift at RRDE or for $\Delta E_{j=2}$ at A-GDE cell measurements (Table 1, entry 8). The $\Delta E_{j=2}$ shift is very similar (31 mV) when the AST is performed at 0.6 V vs. RHE (Table 1, entry 7). Also, the current drops at 0.6 vs. RHE expressed in percentage are similar, even if not identical, between G-GDE and A-GDE cells (Table 1). It must be clear that the A-GDE cell set-up and the G-GDE cell use a very different electrode configurations and the

electrode sizes are also different. Thus, it is plausible that there may be differences in performance even when using the same experimental protocol. However, this does not seem to be the case as both setups produce fairly similar results.

With regard to the quantitative evaluation of H_2O_2, every hour the G-GDE cell compartment directly facing the carbon paper was opened to sample the solution, 100 µL was taken and added to Ti(IV) solution and UV-Vis was recorded to calculate H_2O_2 concentration (see SI for detail). From this set of experiments, a FE of 0.3 % (at 0.2 V) was calculated, which is perfectly in line with the amount derived from RRDE analysis and with a rate of production of 8.8 mmol g^{-1} h^{-1}. By the way, it is worth stressing that under this configuration, part of the produced H_2O_2 could be further reduced, and this explains the limiting yield value observed in Figure 7f. AST or H_2O_2 accumulation tests in alkaline media are not reported for G-GDE set-up because not reliable. This is due to the evident flooding of the electrode (crossover of some electrolytes) which made impossible a correct acquisition, analysis, and evaluation of the experimental results. This was an observation made by looking at the gas and the electrolyte chambers, after a certain period of time water started to trespass the carbon paper and catalysts layer and this can only append due to a modification of carbon paper support that tends to flood and lose its hydrophobic properties that avoid the crossover of electrolyte.

Figure 7g compares the current profiles normalized for both the surface area and loading of the three setups and Table 1 resumes some parameters. The activity recorded in RRDE configuration is superimposable to the one from A-GDE and G-GDE in the region 0.6-0.8 V vs. RHE. At 0.6 V vs RHE, the RRDE disc current reaches its limiting value, while at both GDE setups, the current grows indefinitely due to the absence of the limit of diffusion, which is the exact peculiarity of GDE. An almost identical behavior is observed in the KOH electrolyte, but with all values shifted towards a more positive potential, as generally observed for Fe-N-C. To obtain such coherent results, the catalyst casting need to be done with a single drop than by spray coating and the utilization of a mesoporous carbon layer on top of carbon paper further help (Figure S8), while the cell configuration

does not impact the results (membrane presence and position, arrangement of the reference electrode, etc.).

Figure 7h reports the Tafel plot for the three different setups and the mass transfer corrected Tafel plot for the current profile acquired at RRDE. It is worth stressing that the A-GDE cell and RRDE mass transfer corrected responses have similar even if not identical profiles, confirming how the two techniques can be interchangeable for kinetic analysis. Similar considerations apply to the G-GDE set-up, albeit requiring greater attention in electrode preparation to ensure that the activity of the material is not underestimated (Figure 7g and h and Figure S8). As previously remarked, possible interfering effects are mainly linked to hydrophobicity and therefore bad wettability of the electrode. Furthermore, the G-GDE cell behavior is a setup that could help in the quantitative analysis of FE and product or by-product generation

4 Conclusion

The main conclusions of the present investigation are resumed as follows:

- The effect of catalyst loading on the RRDE electrode had little impact on the mass-normalized kinetic current, which settled at an average value just below 2 A g^{-1}. However, the kinetic current density (current normalized by apparent or geometric surface area) increased as the catalyst loading increased.
- Similar behavior to RRDE was observed in the A-GDE cell, where the kinetic current density also increased with increasing loading, while the mass normalized kinetic current settled at an average value slightly higher than 2 A g^{-1}, excluding the lowest loadings.
- For all the electrochemical set-up (RRDE, A-GDE and G-GDE cell), both the kinetic current density and the mass normalized kinetic current increase at the increase of the loading.

- NO stripping measurements for Fe-N_x sites determination do not show a sensitive dependence from the loading so that the site per unit area is almost constant in this range of 0.2 to 0.8 mg cm^{-2}
- The ORR activity from both RRDE and A-GDE measurements at different pH values in terms of half-wave potential and potential at 10 mA cm^{-2}, respectively, are fully in the agreement. This suggests a definite and absolute interchangeability between the two techniques.
- Comparing the results of AST (7000 cycles between 0.55 and 1.05 V vs. RHE) conducted on RRDE and A-GDE, it is evident that the two methods yield different outcomes. In the former, the electrocatalyst undergoes degradation and loses a portion of its active sites, while in the latter, the electrocatalyst remains stable. These findings suggest that utilizing repeated cycles is not an effective means of stressing GDEs when the nafion membrane is set right over the GDE.
- Chronoamperometry AST, conducted for 8 hours under oxygen flow at either 0.2 V or 0.6 V vs. RHE, resulted in a GDE electrode degradation comparable to that observed by cycling the RRDE. This degradation was also confirmed in the G-GDE electrode. Therefore, it is necessary to utilize distinct and reliable degradation tests when using RRDE or GDE electrodes.
- H_2O_2 yields determined at RRDE and G-GDE cells are fully in accordance.
- Potential-current profile normalized by geometric surface and loading perfectly match among the three different setups even if post iR compensation needs to be considered when high currects flow especially at G-GDE.
- Mass transfer corrected Tafel plot at RRDE and Tafel profile at A-GDE are almost superimposable provided the ink formulation and casting is optimized for the three different set-up

- G-GDE cell can be used for quantitative analysis of FE and generation of products or by-products, but also for kinetic analysis as for RRDE and A-GDE, provided a suitable ink catalyst casting procedure is refined.
- A single technique hardly allows to obtain results that have absolute value. The use of at least two techniques such as RRDE and A-GDE allows a cross cheching of the data obtained as a function of the optimise ink preparation and casting.

Declaration of Competing Interest

The authors declare that they have no known competing financial interests or personal relationships that could have appeared to influence the work reported in this paper.

Credit authorship contribution statement

Marco Mazzucato: Project administration, Formal analysis, Writing – original draft, Conceptualization.

Christian Durante: Revision, Writing –review & editing, project administration.

Acknowledgements

The authors gratefully acknowledge the University of Padova and the Chemical Sciences Department for the financial support through a P-DISC Grant (Project No. P-DiSC#03NExuS_BIRD2021-UNIPD).

5 References

[1] M. Mazzucato, C. Durante, Insights on Oxygen Reduction Reaction to H_2O_2: The role of functional groups and textural properties on the activity and selectivity of doped carbon electrocatalysts, Curr. Opin. Electrochem. 35 (2022) 101051. https://doi.org/10.1016/j.coelec.2022.101051.

[2] K. Ehelebe, T. Ashraf, S. Hager, D. Seeberger, S. Thiele, S. Cherevko, Fuel cell catalyst layer evaluation using a gas diffusion electrode half-cell: Oxygen reduction reaction on Fe-N-C in alkaline media, Electrochem. Commun. 116 (2020) 106761. https://doi.org/10.1016/j.elecom.2020.106761.

[3] L. Bouleau, S. Pérez-Rodríguez, J. Quílez-Bermejo, M.T. Izquierdo, F. Xu, V. Fierro, A. Celzard, Best practices for ORR performance evaluation of metal-free porous carbon electrocatalysts, Carbon 189 (2022) 349–361. https://doi.org/10.1016/j.carbon.2021.12.078.

[4] S.S. Kocha, K. Shinozaki, J.W. Zack, D.J. Myers, N.N. Kariuki, T. Nowicki, V. Stamenkovic, Y. Kang, D. Li, D. Papageorgopoulos, Best Practices and Testing Protocols for Benchmarking ORR Activities of Fuel Cell Electrocatalysts Using Rotating Disk Electrode, Electrocatalysis. 8 (2017) 366–374. https://doi.org/10.1007/s12678-017-0378-6.

[5] H.A. Gasteiger, S.S. Kocha, B. Sompalli, F.T. Wagner, Activity benchmarks and requirements for Pt, Pt-alloy, and non-Pt oxygen reduction catalysts for PEMFCs, Appl. Catal. B Environ. 56 (2005) 9–35. https://doi.org/10.1016/j.apcatb.2004.06.021.

[6] Y. Garsany, J. Ge, J. St-Pierre, R. Rocheleau, K.E. Swider-Lyons, Analytical Procedure for Accurate Comparison of Rotating Disk Electrode Results for the Oxygen Reduction Activity of Pt/C, J. Electrochem. Soc. 161 (2014) F628–F640. https://doi.org/10.1149/2.036405jes.

[7] Y. Garsany, O. a Baturina, K.E. Swider-Lyons, S.S. Kocha, Experimental methods for quantifying the activity of platinum electrocatalysts for the oxygen reduction reaction, Anal. Chem. 82 (2010) 6321–6328. https://doi.org/10.1021/ac100306c.

[8] H. Zhang, L. Osmieri, J.H. Park, H.T. Chung, D.A. Cullen, K.C. Neyerlin, D.J. Myers, P. Zelenay, Standardized protocols for evaluating platinum group metal-free oxygen reduction reaction electrocatalysts in polymer electrolyte fuel cells, Nat. Catal. 5 (2022) 455–462. https://doi.org/10.1038/s41929-022-00778-3.

[9] C.M. Zalitis, D. Kramer, A.R. Kucernak, Electrocatalytic performance of fuel cell reactions at low catalyst loading and high mass transport, Phys. Chem. Chem. Phys. 15 (2013) 4329. https://doi.org/10.1039/c3cp44431g.

[10] M. Inaba, A.W. Jensen, G.W. Sievers, M. Escudero-Escribano, A. Zana, M. Arenz, Benchmarking high surface area electrocatalysts in a gas diffusion electrode: measurement of oxygen reduction activities under realistic conditions, Energy Environ. Sci. 11 (2018) 988–994. https://doi.org/10.1039/C8EE00019K.

[11] K. Ehelebe, N. Schmitt, G. Sievers, A.W. Jensen, A. Hrnjić, P. Collantes Jiménez, P. Kaiser, M. Geuß, Y.-P. Ku, P. Jovanovič, K.J.J. Mayrhofer, B. Etzold, N. Hodnik, M. Escudero-Escribano, M. Arenz, S. Cherevko, Benchmarking Fuel Cell Electrocatalysts Using Gas Diffusion Electrodes: Inter-lab Comparison and Best Practices, ACS Energy Lett. 7 (2022) 816–826. https://doi.org/10.1021/acsenergylett.1c02659.

[12] R. Riasse, C. Lafforgue, F. Vandenberghe, F. Micoud, A. Morin, M. Arenz, J. Durst, M. Chatenet, Benchmarking proton exchange membrane fuel cell cathode catalyst at high current density: A comparison between the rotating disk electrode, the gas diffusion electrode and differential cell, J. Power Sources. 556 (2023). https://doi.org/10.1016/j.jpowsour.2022.232491.

[13] S. Alinejad, M. Inaba, J. Schröder, J. Du, J. Quinson, A. Zana, M. Arenz, Testing fuel cell catalysts under more realistic reaction conditions: accelerated stress tests in a gas diffusion electrode setup, J.Phys Energy. 2 (2020). https://doi.org/10.1088/2515-7655/ab67e2.

[14] G.W. Sievers, A.W. Jensen, V. Brüser, M. Arenz, M. Escudero-Escribano, Sputtered Platinum Thin-films for Oxygen Reduction in Gas Diffusion Electrodes: A Model System for Studies

under Realistic Reaction Conditions, Surfaces. 2 (2019) 336–348. https://doi.org/10.3390/surfaces2020025.

[15] M. Mazzucato, L. Gavioli, V. Balzano, E. Berretti, G.A. Rizzi, D. Badocco, P. Pastore, A. Zitolo, C. Durante, Synergistic Effect of Sn and Fe in Fe–N_x Site Formation and Activity in Fe–N–C Catalyst for ORR, ACS Appl. Mater. Interfaces. 14 (2022) 54635–54648. https://doi.org/10.1021/acsami.2c13837.

[16] M. Mazzucato, C. Durante, How determinant is the iron precursor ligand in Fe-N-C single-site formation and activity for oxygen reduction reaction?, Electrochim. Acta. 394 (2021) 139105. https://doi.org/10.1016/j.electacta.2021.139105.

[17] D. Malko, A. Kucernak, T. Lopes, In situ electrochemical quantification of active sites in Fe–N/C non-precious metal catalysts, Nat. Commun. 7 (2016) 13285–13291. https://doi.org/10.1038/ncomms13285.

[18] V.C.A. Ficca, C. Santoro, E. Placidi, F. Arciprete, A. Serov, P. Atanassov, B. Mecheri, Exchange Current Density as an Effective Descriptor of Poisoning of Active Sites in Platinum Group Metal-free Electrocatalysts for Oxygen Reduction Reaction, ACS Catal. 13 (2023) 2162–2175. https://doi.org/10.1021/acscatal.2c05222.

[19] M.W. Chung, G. Chon, H. Kim, F. Jaouen, C.H. Choi, Electrochemical Evidence for Two Sub-families of FeN_xC_y Moieties with Concentration-Dependent Cyanide Poisoning, ChemElectroChem. 5 (2018) 1880–1885. https://doi.org/10.1002/celc.201800067.

[20] M.S. Thorum, J.M. Hankett, A.A. Gewirth, Poisoning the oxygen reduction reaction on carbon-supported Fe and Cu electrocatalysts: Evidence for metal-centered activity, J. Phys. Chem. Lett. 2 (2011) 295–298. https://doi.org/10.1021/jz1016284.

[21] N.R. Sahraie, U.I. Kramm, J. Steinberg, Y. Zhang, A. Thomas, T. Reier, J.P. Paraknowitsch, P. Strasser, Quantifying the density and utilization of active sites in non-precious metal oxygen electroreduction catalysts, Nat. Commun. 6 (2015) 1–9. https://doi.org/10.1038/ncomms9618.

[22] M. Primbs, Y. Sun, A. Roy, D. Malko, A. Mehmood, M.-T. Sougrati, P.-Y. Blanchard, G.

Granozzi, T. Kosmala, G. Daniel, P. Atanassov, J. Sharman, C. Durante, A. Kucernak, D. Jones, F. Jaouen, P. Strasser, Establishing reactivity descriptors for platinum group metal (PGM)-free Fe–N–C catalysts for PEM fuel cells, Energy Environ. Sci. 13 (2020) 2480–2500. https://doi.org/10.1039/D0EE01013H.

[23] D. Malko, A. Kucernak, T. Lopes, Performance of Fe–N/C Oxygen Reduction Electrocatalysts toward NO_2^- , NO, and NH_2OH Electroreduction: From Fundamental Insights into the Active Center to a New Method for Environmental Nitrite Destruction, J. Am. Chem. Soc. 138 (2016) 16056–16068. https://doi.org/10.1021/jacs.6b09622.

[24] G. Daniel, M. Mazzucato, R. Brandiele, L. De Lazzari, D. Badocco, P. Pastore, T. Kosmala, G. Granozzi, C. Durante, Sulfur Doping versus Hierarchical Pore Structure: The Dominating Effect on the Fe–N–C Site Density, Activity, and Selectivity in Oxygen Reduction Reaction Electrocatalysis, ACS Appl. Mater. Interfaces. 13 (2021) 42693–42705. https://doi.org/10.1021/acsami.1c09659.

[25] M. Mazzucato, G. Daniel, A. Mehmood, T. Kosmala, G. Granozzi, A. Kucernak, C. Durante, Effects of the induced micro- and meso-porosity on the single site density and turn over frequency of Fe-N-C carbon electrodes for the oxygen reduction reaction, Appl. Catal. B Environ. 291 (2021) 120068–120083. https://doi.org/10.1016/j.apcatb.2021.120068.

[26] K. Kumar, L. Dubau, M. Mermoux, J. Li, A. Zitolo, J. Nelayah, F. Jaouen, F. Maillard, On the Influence of Oxygen on the Degradation of Fe-N-C Catalysts, Angew. Chemie. 132 (2020) 3261–3269. https://doi.org/10.1002/ange.201912451.

[27] A. Goyal, G. Marcandalli, V.A. Mints, M.T.M. Koper, Competition between CO_2 Reduction and Hydrogen Evolution on a Gold Electrode under Well-Defined Mass Transport Conditions, J. Am. Chem. Soc. 142 (2020) 4154–4161. https://doi.org/10.1021/jacs.9b10061.

[28] K.H. Wu, Q. Zhang, Y. Lin, M.A. Ali, S. Zhao, S. Heumann, G. Centi, Real-Time Carbon Monoxide Detection using a Rotating Gold Ring Electrode: A Feasibility Study, ChemElectroChem. 7 (2020) 4417–4422. https://doi.org/10.1002/celc.202001263.

[29] A. Facchin, M. Zerbetto, A. Gennaro, A. Vittadini, D. Forrer, C. Durante, Oxygen Reduction Reaction at Single-Site Catalysts: A Combined Electrochemical Scanning Tunnelling Microscopy and DFT Investigation on Iron Octaethylporphyrin Chloride on HOPG, ChemElectroChem. 8 (2021) 2825–2835. https://doi.org/10.1002/celc.202100543.

[30] X. Xie, C. He, B. Li, Y. He, D.A. Cullen, E.C. Wegener, A.J. Kropf, U. Martinez, Y. Cheng, M.H. Engelhard, M.E. Bowden, M. Song, T. Lemmon, X.S. Li, Z. Nie, J. Liu, D.J. Myers, P. Zelenay, G. Wang, G. Wu, V. Ramani, Y. Shao, Performance enhancement and degradation mechanism identification of a single-atom Co–N–C catalyst for proton exchange membrane fuel cells, Nat. Catal. 3 (2020) 1044–1054. https://doi.org/10.1038/s41929-020-00546-1.

[31] A. Ohma, K. Shinohara, A. Iiyama, T. Yoshida, A. Daimaru, Membrane and Catalyst Performance Targets for Automotive Fuel Cells by FCCJ Membrane, Catalyst, MEA WG, ECS Trans. 41 (2019) 775–784. https://doi.org/10.1149/1.3635611.

[32] F. Luo, A. Roy, L. Silvioli, D.A. Cullen, A. Zitolo, M.T. Sougrati, I.C. Oguz, T. Mineva, D. Teschner, S. Wagner, J. Wen, F. Dionigi, U.I. Kramm, J. Rossmeisl, F. Jaouen, P. Strasser, P-block single-metal-site tin/nitrogen-doped carbon fuel cell cathode catalyst for oxygen reduction reaction, Nat. Mater. 19 (2020) 1215–1223. https://doi.org/10.1038/s41563-020-0717-5.

[33] S.H. Lee, J. Kim, D.Y. Chung, J.M. Yoo, H.S. Lee, M.J. Kim, B.S. Mun, S.G. Kwon, Y.-E. Sung, T. Hyeon, Design Principle of Fe–N–C Electrocatalysts: How to Optimize Multimodal Porous Structures?, J. Am. Chem. Soc. 141 (2019) 2035–2045. https://doi.org/10.1021/jacs.8b11129.

[34] J. Li, S. Chen, N. Yang, M. Deng, S. Ibraheem, J. Deng, J. Li, Ultrahigh-Loading Zinc Single-Atom Catalyst for Highly Efficient Oxygen Reduction in Both Acidic and Alkaline Media Angew. Chem. Int. Ed., (2019) 7035–7039. https://doi.org/10.1002/anie.201902109.

[35] W.J. Jiang, L. Gu, L. Li, Y. Zhang, X. Zhang, L.J. Zhang, J.Q. Wang, J.S. Hu, Z. Wei, L.J. Wan, Understanding the High Activity of Fe-N-C Electrocatalysts in Oxygen Reduction:

Fe/Fe_3C Nanoparticles Boost the Activity of Fe-N_x, J. Am. Chem. Soc. 138 (2016) 3570–3578. https://doi.org/10.1021/jacs.6b00757.

[36] J. Schröder, V.A. Mints, A. Bornet, E. Berner, M. Fathi Tovini, J. Quinson, G.K.H. Wiberg, F. Bizzotto, H.A. El-Sayed, M. Arenz, The Gas Diffusion Electrode Setup as Straightforward Testing Device for Proton Exchange Membrane Water Electrolyzer Catalysts, J. Am. Chem. Soc. 1 (2021) 247–251. https://doi.org/10.1021/jacsau.1c00015.

[37] S. Alinejad, J. Quinson, J. Schröder, J.J.K. Kirkensgaard, M. Arenz, Carbon-Supported Platinum Electrocatalysts Probed in a Gas Diffusion Setup with Alkaline Environment: How Particle Size and Mesoscopic Environment Influence the Degradation Mechanism, ACS Catal. 10 (2020) 13040–13049. https://doi.org/10.1021/acscatal.0c03184.

[38] M. De Jesus Gálvez-Vázquez, P. Moreno-García, H. Xu, Y. Hou, H. Hu, I.Z. Montiel, A. V. Rudnev, S. Alinejad, V. Grozovski, B.J. Wiley, M. Arenz, P. Broekmann, P. Moreno-García, Environment Matters: CO2RR Electrocatalyst Performance Testing in a Gas-Fed Zero-Gap Electrolyzer, ACS Catal. 10 (2020) 13096–13108. https://doi.org/10.1021/acscatal.0c03609.

[39] A. Bonakdarpour, M. Lefevre, R. Yang, F. Jaouen, T. Dahn, J.-P. Dodelet, J.R. Dahn, Impact of Loading in RRDE Experiments on Fe–N–C Catalysts: Two- or Four-Electron Oxygen Reduction?, Electrochem. Solid-State Lett. 11 (2008) B105. https://doi.org/10.1149/1.2904768.

[40] S. Trasatti, O.A. Petrii, Real surface area measurements in Electrochemistry, J. Electroanal. Chem. 327 (1992) 353–376.

[41] S. Rojas-Carbonell, K. Artyushkova, A. Serov, C. Santoro, I. Matanovic, P. Atanassov, Effect of pH on the Activity of Platinum Group Metal-Free Catalysts in Oxygen Reduction Reaction, ACS Catal. 8 (2018) 3041–3053. https://doi.org/10.1021/acscatal.7b03991.

[42] S. Brocato, A. Serov, P. Atanassov, pH dependence of catalytic activity for ORR of the non-PGM catalyst derived from heat-treated Fe–phenanthroline, Electrochim. Acta. 87 (2013) 361–365. https://doi.org/10.1016/j.electacta.2012.09.053.

[43] K. Wan, Z. Yu, X. Li, M. Liu, G. Yang, J. Piao, Z. Liang, pH Effect on Electrochemistry of Nitrogen-Doped Carbon Catalyst for Oxygen Reduction Reaction, ACS Catal. (2015) 150601163235008. https://doi.org/10.1021/acscatal.5b01089.

[44] V. Perazzolo, E. Grądzka, C. Durante, R. Pilot, N. Vicentini, G.A. Rizzi, G. Granozzi, A. Gennaro, Chemical and electrochemical stability of nitrogen and sulphur doped mesoporous carbons, Electrochim. Acta. 197 (2016) 251–262. https://doi.org/10.1016/j.electacta.2016.02.025.